

Original article

3D-QSAR studies of triazafluorenone inhibitors of metabotropic glutamate receptor subtype 1

Y. Nataraja Sekhar, Muttineni Ravikumar*, M. Ravi Shashi Nayana, Shyam C. Mallena, Madala Kishore Kumar

Biocampus, S-1, Phase-I Technocrats Industrial Estate, Balanagar, Hyderabad 500 037, Andhra Pradesh, India

Received 24 January 2007; received in revised form 16 June 2007; accepted 21 June 2007

Available online 14 July 2007

Abstract

Three-dimensional quantitative structure-activity relationship (3D-QSAR) models were developed for 46 triazafluorenone derivatives, inhibiting metabotropic glutamate receptor subtype 1 (mGluR1). It includes molecular field analysis (MFA) and receptor surface analysis (RSA). The QSAR model was developed using 35 compounds and its predictive ability was assessed using a test set of 11 compounds. The predictive 3D-QSAR models have conventional r^2 values of 0.908 and 0.798 for MFA and RSA, respectively; while the cross-validated coefficient r_{cv}^2 values of 0.707 and 0.580 for MFA and RSA, respectively. The results of 3D-QSAR methodologies provide a powerful tool directed to the design of novel and selective triazafluorenone inhibitors.

© 2007 Elsevier Masson SAS. All rights reserved.

Keywords: 3D-QSAR; MFA; RSA; mGluR1; Triazafluorenone inhibitors**1. Introduction**

Metabotropic glutamate receptors (mGluRs) are a class of G-protein coupled receptors that possess seven transmembrane regions and couple with a variety of second messenger systems, including the activation of phosphoinositide hydrolysis and the regulation of adenylyl cyclase [1–3]. There are three different groups, group I, II, and III, of mGluRs with a total of eight distinct subtypes, mGluR1–mGluR8, based on their primary sequence similarity, signal transduction linkages, and pharmacological profile [4]. Groups I mGluRs, mGluR1 and mGluR5, play key roles in the central sensitization of pain, in addition to a variety of functions with potential implications in neurological and psychiatric disorders [5]. The group I receptors are coupled to Gq/11, and activation of these receptors stimulates phospholipase C, which hydrolyses phosphatidyl inositol-4,5-bisphosphate into

inositol trisphosphate (IP3) and diacylglycerol. IP3 in turn binds to the IP3 receptor on the endoplasmic reticulum, evoking a release of Ca^{2+} from these intracellular stores. Ca^{2+} and diacylglycerol activate protein kinase C. Group II and group III receptors are coupled to Gi, and activation of the receptors leads to an inhibition of adenylyl cyclase, thereby inhibiting intracellular cAMP formation and protein kinase A activation [6]. mGluRs modulate pain transmission in the spinal cord, most likely via sensitization of dorsal horn neurons to sustain high-intensity C-fiber input. Normalization of glutamatergic neurotransmission in the spinal cord and nociceptive afferents via inhibition of the group I mGluRs is manifested in the attenuation of pain [7].

There are several competitive and noncompetitive inhibitors, shows activity on mGluR1, reported in literature. The first reported noncompetitive, non-amino acid-like mGluR1 antagonist, CPCCOEt (7-hydroxyimino)cyclopropa[b]chromen-1a-carboxylate ethyl ester [a, Fig. 1], elucidated an allosteric binding site for the target [8]. Other noncompetitive inhibitors are BAY 36-7620 (b), thiazolo[3,2-*a*]benzimidazole-2-carboxamide 19 derivatives (c), NPS-2390 (d), azepinyl

* Corresponding author. Tel.: +91 09989889074.

E-mail address: ravambio@gmail.com (M. Ravikumar).

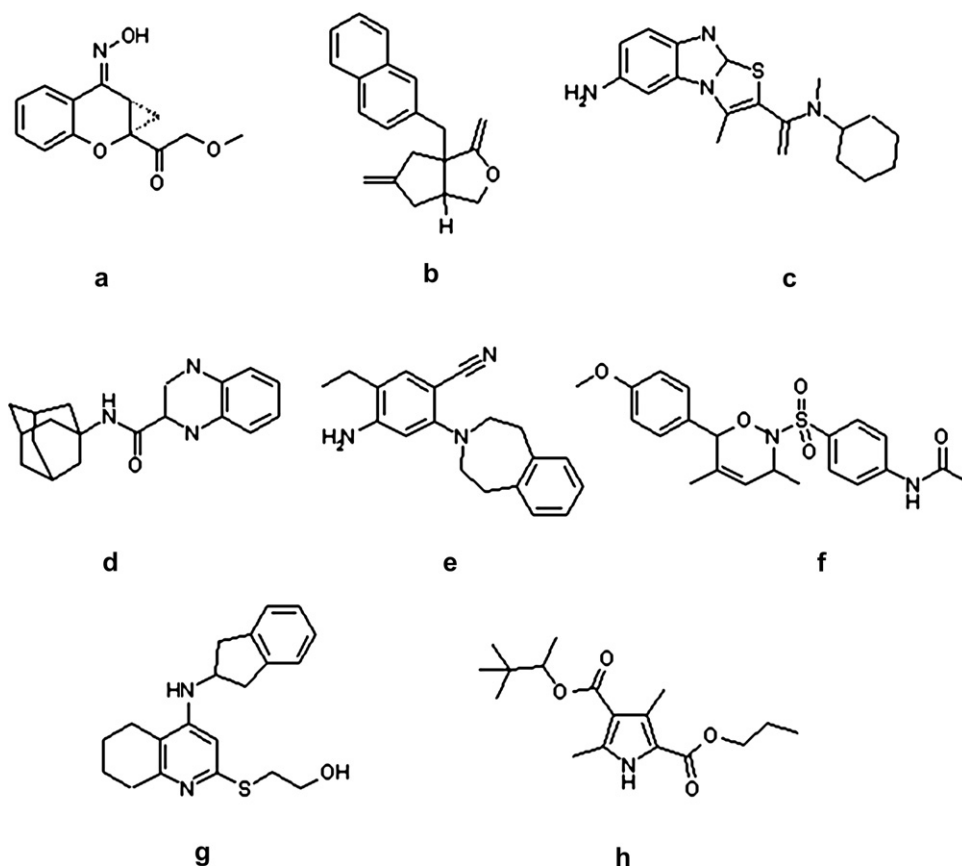


Fig. 1. Structures of known noncompetitive mGluR1 antagonists.

derivatives (e), oxazine derivatives (f), 4-amino-5,6,7,8-tetrahydroquinazoline derivative (g) and PPP-1 (h), given in literature [9–15]. Recently a set of potent noncompetitive triazafluorenone inhibitors were prepared [16,17], these compounds were considered for our present study.

In the current study, we have performed 3D-QSAR studies including molecular field analysis (MFA) and receptor surface analysis (RSA), which may serve as a useful tool to gain insight into the mechanism of inhibition and to predict the inhibitory properties of newly designed triazafluorenone analogues. This is the first study aimed at deriving predictive 3D-QSAR models for mGluR1 inhibitors.

2. Experimental methods

2.1. Data set and molecular modeling

A data set of 46 triazafluorenone derivatives [16,17] reported to have rat group 1 metabotropic glutamate receptor (mGluR1) inhibitory activities was used for the present 3D-QSAR (MFA and RSA) studies (Table 1). *In vitro* inhibitory concentrations (IC_{50}) of the molecules against mGluR1 were converted into corresponding pIC_{50} ($-\log IC_{50}$) and used as dependent variables in the 3D-QSAR calculations. The total set of inhibitors was divided into a training set (35 compounds) for generating 3D-QSAR model and a test set (11 compounds) for validating the quality of the models.

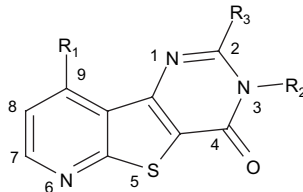
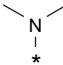
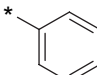
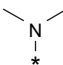
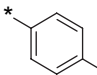
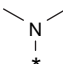
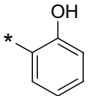
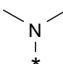
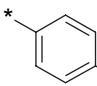
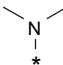
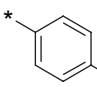
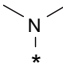
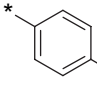
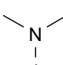
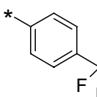
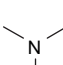
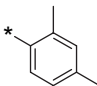
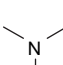
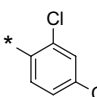
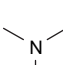
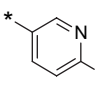
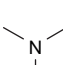
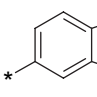
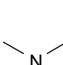
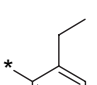
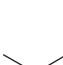
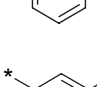
The training and test sets' selections were done manually so that structurally diverse molecules possessing activities of wide range were included in both sets (Table 1).

Three-dimensional structures of all triazafluorenone derivatives were constructed by using *Cerius*² Version 4.10 [19] on silicon graphics workstation. Energy minimization was performed by OFF methods using the steepest descent algorithm with a convergence criterion of 0.001 kcal/mol. Partial atomic charges were calculated using the Gasteiger method [20]. Further geometry optimization of each molecule was carried out with MOPAC 6 package using the semi-empirical AM1 Hamiltonian.

2.2. Alignment procedure

The alignment was carried out using the shape reference alignment option in the QSAR module within *Cerius*². This option uses MCS (maximum common subgraph) method for alignment of structures through pair-wise atom superpositioning, places all structures in the study table in the same frame of reference as the shape reference compound. The MCS method looks at molecules as points and lines and uses the techniques of graph theory to identify patterns. It finds the largest subset of atoms in the shape reference compound that is shared by all structures in the study table and uses this subset for alignment. A rigid fit of atom pairings was performed to superimpose each structure so that it overlays the shape reference

Table 1
Structures and biological activities of molecules used for the present study

Compound	Structure			IC ₅₀ (nM)	pIC ₅₀
	R ₁	R ₂	R ₃		
					
1			—	20	7.699
2			—	5	8.301
3			—	50	7.301
4			—	23	7.638
5			—	16	7.796
6			—	4	8.398
7			—	32	7.495
8			—	17	7.770
9			—	45	7.347
10			—	39	7.409
11			—	122	6.914
12			—	251	6.600
13			—	9	8.046

(continued on next page)

Table 1 (continued)

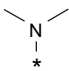
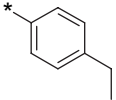
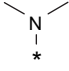
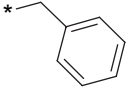
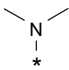
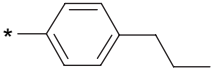
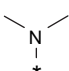
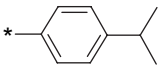
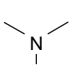
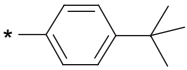
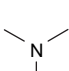
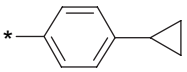
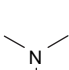
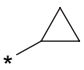
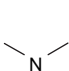
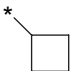
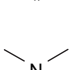
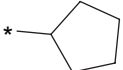
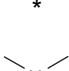
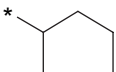
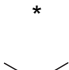
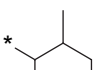
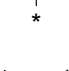
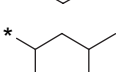
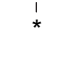
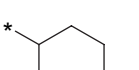
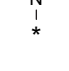
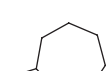
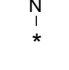
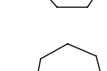
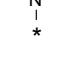
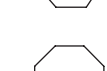
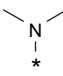
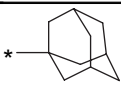
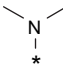
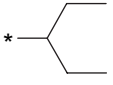
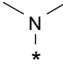
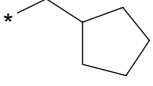
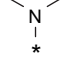
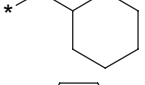
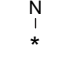
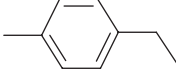
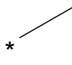
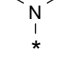
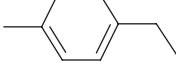
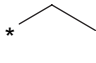
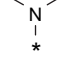
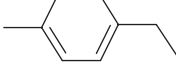

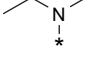
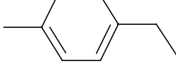
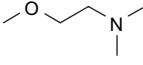
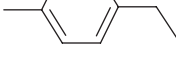
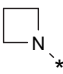
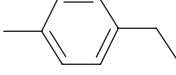
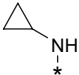
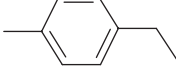
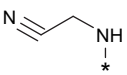
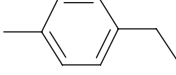
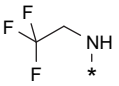
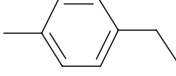
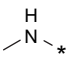
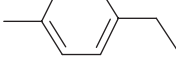
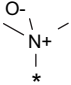
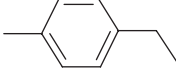
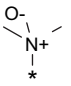
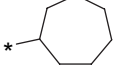
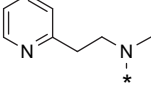
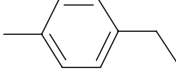
Compound	Structure			IC ₅₀ (nM)	pIC ₅₀
	R ₁	R ₂	R ₃		
14			—	3	8.523
15			—	281	6.551
16			—	180	6.745
17			—	407	6.390
18			—	8500	5.071
19			—	87	7.060
20			—	632	6.199
21			—	167	6.777
22			—	5	8.301
23			—	50	7.301
24			—	130	6.886
25			—	482	6.317
26			—	140	6.854
27			—	1	9.000
28			—	10	8.000
29			—	13	7.886

Table 1 (continued)

Compound	Structure			IC ₅₀ (nM)	pIC ₅₀
	R ₁	R ₂	R ₃		
30			—	76	7.119
31			—	335	6.475
32			—	26	7.585
33			—	139	6.857
34				44	7.357
35				84	7.076
36				101	6.996
37			—	37	7.432
38			—	71	7.149
39			—	113	6.947
40			—	41	7.387
41			—	49	7.370
42			—	99	7.004
43			—	98	7.009
44			—	306	6.514
45			—	167	6.777
46			—	52	7.284

compound. The most active compound **27** was used as shape reference compound for superposing the rest of the molecules. The aligned molecules are shown in Fig. 2.

2.3. QSAR studies

2.3.1. Molecular field analysis (MFA)

MFA studies were performed using the QSAR module of Cerius² [19,21]. MFA quantifies the interaction energy between a probe molecule in the molecular field and a set of aligned target molecules in a QSAR. Interaction energies measured and analyzed for a set of 3D structures can be useful in establishing QSARs. The molecular field was created using proton and methyl groups as probes, which represent electrostatic and steric fields, respectively. These fields were sampled at each point of a regularly spaced grid of 1 Å. An energy cut-off of ± 30.0 kcal/mol was set for both steric and electrostatic and the total grid points generated were 1245. In addition, the number of spatial and structural descriptors such as polarizability, dipole moment, radius of gyration, number of rotatable bonds, molecular volume, principle moments of inertia, $A \log P$, number of hydrogen bond donors and acceptors, and molar refractivity were considered along with the steric and electrostatic descriptors. Only 10% of the total descriptors for which the variance was the highest were considered for further analysis. Regression analysis was carried out using the genetic partial least squares (G/PLS) method consisting of 50,000 generations with a population size of 100. The optimum number of components was set to 5. The smoothing parameter, d , was set to 1.0 to control the bias in the scoring factors between equations with different number of terms. Cross-validation was performed with the leave-one-out procedure. PLS analysis was scaled, with all variables normalized to a variance of 1.0.

2.3.2. Receptor surface analysis

A receptor surface model represents essential information about the hypothetical receptor site as a three-dimensional surface with associated properties mapped onto the surface model. The same set of aligned molecules was considered for the generation of a receptor surface, using the van der Waals field

function. The contribution of each molecule in the generation of receptor surface is proportional to its biological activity. The most active compounds **27**, **6**, **22**, **2**, **13** and **28** with the activity ranging from 1 nM to 10 nM, were used to develop the Receptor Surface Model (RSM). During this process, various chemical properties, namely charge, electrostatic potential, hydrogen bonding propensity and hydrophobicity associated with each surface point were calculated automatically. Each molecule was docked into this generated receptor. The interaction energy and strain energy between the molecule and the receptor was evaluated and added to the study table. Further, the interaction energies of each molecule with different probes such as methyl group (steric) and a proton (electrostatic) positioned along the grid points throughout the receptor surface were added to the study table. Only 10% of the total descriptors whose variance was highest were considered as independent data to perform further analysis. Regression analysis was carried out using the G/PLS method as mentioned above.

3. Results and discussion

3.1. Molecular field analysis

Molecular field analysis model was derived using series of triazafluorenone derivatives having mGluR1 inhibitory activities [Table 1]. The training set consisted of 35 compounds while the model was validated using an external set of 11 compounds. The statistical details of the MFA model are shown in Table 4 ($r^2 = 0.908$, $r_{cv}^2 = 0.707$). Tables 2 and 3 show the actual and predicted activities obtained from MFA model for the training and the test set molecules, respectively. Fig. 4 shows the graph of actual versus predicted pIC₅₀ values of the training set and the test set molecules for MFA model.

The cross-validated r_{cv}^2 for MFA model was 0.707, while the non-cross-validated r^2 with five components was 0.908. The bootstrapping r_{bs}^2 value was 0.855. The QSAR equation of MFA model is described below. The steric (CH₃) and electrostatic (H⁺) descriptors in the equations specify the regions where structural variations in the ligands result in variation of the biological activity (Fig. 3). The electrostatic descriptor H⁺ with positive coefficient indicates a region favorable for electropositive group, while negative coefficient indicates electronegative (electron-withdrawing) group required at the position. The numbers associated with the descriptor specify its location in the 3D-grid around the molecule. The equation generated by MFA model is given by the following Eq. (1)

$$\begin{aligned} \text{Activity} = & 8.28719 + 0.024478(\text{H} + /397) \\ & + 0.064294(\text{CH}_3/540) - 0.019478(\text{H} + /460) \\ & - 0.027944(\text{CH}_3/590) + 0.033213(\text{CH}_3/542) \\ & - 0.04022(\text{CH}_3/549) - 0.000197('Apo'') \\ & + 0.029841(\text{H} + /163) \end{aligned} \quad (1)$$

Presence of electrostatic descriptor (H⁺/163) at C⁹ position of 5-thia-1,3,6-triazafluorenone indicates that the importance

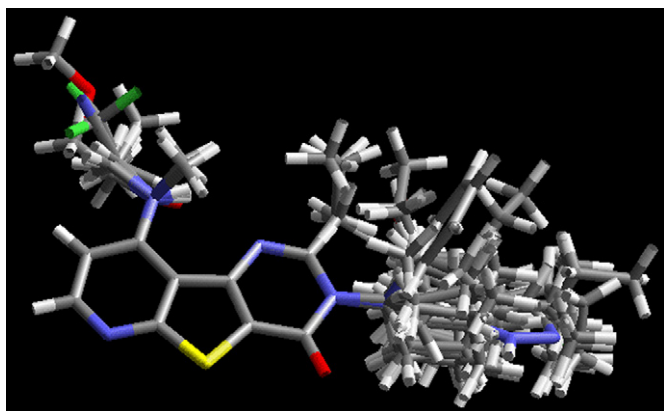


Fig. 2. Alignment of all molecules used for molecular field generation.

Table 2
Actual and predicted activities of the training set molecules by the MFA and RSA models

Compound	pIC ₅₀				
	Exp.	MFA		RSA	
		Predicted	Residual	Predicted	Residual
2	8.301	8.102	0.199	7.739	0.562
4	7.638	7.566	0.072	7.831	−0.193
5	7.796	8.097	−0.301	7.926	−0.130
6	8.398	8.358	0.04	7.930	0.468
7	7.495	7.548	−0.053	7.777	−0.282
8	7.770	7.927	−0.157	7.622	0.147
10	7.409	7.401	0.008	6.821	0.588
11	6.914	7.117	−0.203	6.727	0.187
12	6.600	6.953	−0.353	7.502	−0.902
13	8.046	8.070	−0.024	8.104	−0.058
16	6.745	6.352	0.393	7.040	−0.296
17	6.390	6.380	0.01	6.575	−0.184
18	5.071	5.484	−0.413	5.466	−0.395
19	7.060	7.108	−0.048	6.849	0.211
20	6.199	6.437	−0.238	6.494	−0.295
21	6.777	6.680	0.097	6.410	0.368
22	8.301	8.248	0.053	8.215	0.086
23	7.301	7.090	0.211	7.086	0.215
24	6.886	6.975	−0.089	7.267	−0.381
27	9.000	8.945	0.055	8.778	0.222
29	7.886	7.685	0.201	8.070	−0.184
30	7.119	7.416	−0.297	7.693	−0.574
31	6.475	6.146	0.329	6.418	0.057
32	7.585	7.453	0.132	7.544	0.041
33	6.857	6.896	−0.039	6.679	0.178
34	7.357	7.045	0.312	6.887	0.469
36	6.996	6.846	0.15	6.892	0.104
38	7.149	6.854	0.295	7.085	0.064
40	7.387	7.665	−0.278	6.979	0.408
41	7.370	7.165	0.205	7.193	0.117
42	7.004	6.772	0.232	7.330	−0.325
43	7.009	7.164	−0.155	7.067	−0.058
44	6.514	6.764	−0.25	6.732	−0.217
45	6.777	7.159	−0.382	7.030	−0.253
46	7.284	7.124	0.16	7.047	0.237

Table 3
Actual and predicted activities of test set molecules by MFA and RSA models

Compound	pIC ₅₀				
	Exp.	MFA		RSA	
		Predicted	Residual	Predicted	Residual
1	7.699	8.130	−0.431	7.095	0.604
3	7.301	7.042	0.259	7.832	−0.531
9	7.347	7.645	−0.298	7.698	−0.352
14	8.523	8.182	0.341	7.578	0.945
15	6.551	4.967	1.584	6.861	−0.310
25	6.317	7.021	−0.704	6.579	−0.262
26	6.854	7.010	−0.156	6.595	0.259
28	8.000	8.222	−0.222	8.572	−0.572
35	7.076	6.944	0.132	6.880	0.195
37	7.432	7.077	0.355	6.860	0.572
39	6.947	7.663	−0.716	8.152	−1.205

Table 4
Statistical details for MFA and RSA 3D-QSAR models

Component	MFA	RSA
r_{cv}^2 ^a	0.707	0.579
r^2 ^b	0.908	0.798
n ^c	5	5
r_{bs}^2 ^d	0.855	0.719
r_{pred}^2 ^e	0.705	0.776

^a Cross-validated r^2 .

^b Conventional r^2 .

^c Number of components.

^d Bootstrap r^2 .

^e Predictive r^2 .

of the electrostatic environment at this position. Any electron-donating groups at this position could enhance the mGluR1 inhibitory activity. This can be observed in compounds **14**, **37**, **40** and **43**. These molecules contain alkyl amine group at this position and show higher activity than the compound **44**, substituted with electron-withdrawing groups. The presence of steric descriptors (CH₃/542, CH₃/540 and CH₃/590) in the vicinity of the N³ position of pyrimidone ring indicates the importance of steric interactions. CH₃/542, CH₃/540 with positive coefficient and CH₃/590 with negative coefficient indicate that bigger steric group will show negative effect on activity. Cycloheptyl group at this position has highest activity and replacing with cyclopropyl, cyclobutyl, cyclopentyl, cyclohexyl and cyclooctyl decreases its activity. This is evident in the compounds **20–23** and **27–29**. Ethylbenzene at this position have optimum activity compared with phenyl, tolyl and propyl benzene, can be observed in molecules **1**, **2**, **16**. The presence of two electrostatic descriptors at this position with a negative coefficient (H⁺/163) and with a positive coefficient (H⁺/397) describes a subtle balance of electrostatic parameters required at this position. Substitution of bromine in *para*-position to the phenyl group (compound **5**) instead of methyl (compound **2**) at this position improves activity. The moderate electron-withdrawing groups with appropriate steric parameters are need at this position, as trend shown by the molecules **4** < **5** < **6**. The steric descriptor (CH₃/549) with negative coefficient near the C² position of pyrimidone ring indicates that groups with steric group at these position lead to drop in activity. Thus, molecule **1** is having higher activity than **34–36**. The equation also contains an electronic descriptor, Apol, represents the sum of atomic polarizabilities of the molecule,

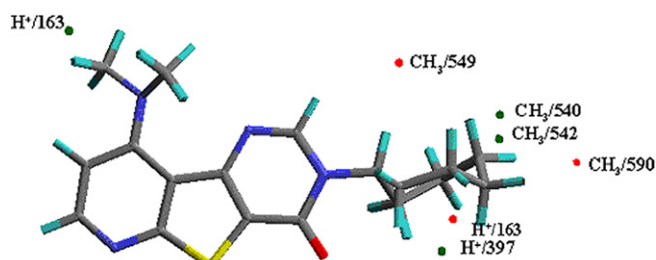


Fig. 3. Compound **27** with 3D points of the QSAR equation. H⁺ represents electrostatic interaction, while CH₃ represents steric interaction.

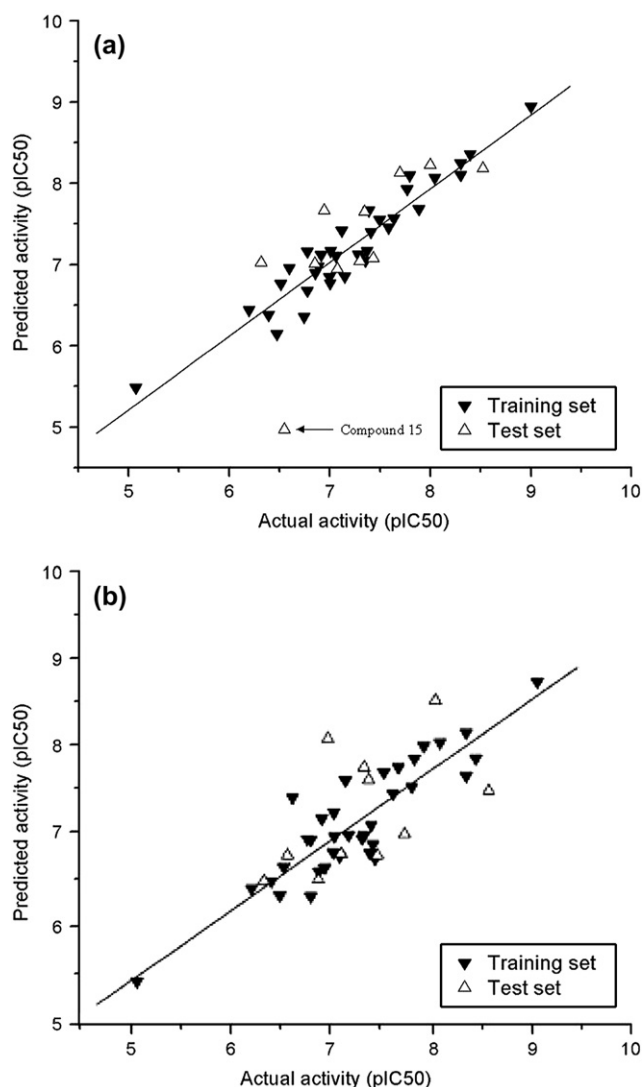


Fig. 4. Graphs of actual versus predicted pIC_{50} for both training and test set molecules for (a) MFA and (b) RSM 3D-QSAR models (outlier labeled).

negative correlation of this term with activity indicates that decrease in the $Apol$ value would result in increase in activity.

A high r_{cv}^2 alone, however, is not a sufficient criterion for a QSAR model to be robust and highly predictive [18]. The predictive power of the model was, therefore validated by using the molecules, not included in the training set and is defined as follows:

$$r_{pred}^2 = (SD - PRESS)/SD \quad (2)$$

where SD is the sum of squared deviations between the biological activities of each molecule and the mean activity of the training set molecules and $PRESS$ is the sum of squared deviations between the predicted and actual activity values for every molecule in the test set. Except compound **15**, remaining 10 molecules in the test set were predicted correctly with an error less than 1.5. Compound **15** was found to be an outlier and its activity is under predicted in MFA. This might be due to the conformational flexibility of methylene group

between triazafluorenone ring and phenyl ring. The orientation of $-CH_2C_6H_5$ group in this molecule is very nearer to the negative coefficient in the equation ($CH_3/590$), hence the activity was under predicted. The predictive r^2 (r_{pred}^2) value was found to be 0.705 without compound **15**. Hence, the predictive ability of MFA model is high except for compound **15**.

3.2. Receptor surface analysis

A receptor surface model was developed using same training set molecules, which are used in MFA studies. The generated model have cross-validated correlation coefficient ($r_{cv}^2 = 0.58$) and conventional r^2 of 0.80. The QSAR equation generated by RSA is given in following equation:

$$\begin{aligned} \text{Activity} = & 2.63756 - 0.877792 \times (\text{ELE}/3282) + 4.31218 \\ & \times (\text{ELE}/2964) + 39.3845 \times (\text{VDW}/877) \\ & - 55.2117 \times (\text{VDW}/871) + 0.716764 \\ & \times (\text{ELE}/2698) - 3.94929 \times (\text{ELE}/2938) \\ & + 4.65262 \times (\text{VDW}/1955) - 17.6025 \\ & \times (\text{VDW}/878) + 42.6652 \times (\text{VDW}/872) \quad (3) \end{aligned}$$

The equation consists of nine receptor field descriptors. The positioning of these descriptors, indicated by a number along with the descriptors, on the model explains the nature of the substituents required. The presence of one negative coefficient steric descriptor ($VDW/878$) and two positive coefficient steric descriptors ($VDW/872$, $VDW/877$) at N^3 position of pyrimidone ring explains the need of a moderately bulky is required at this position. In *para*-substituted phenyl groups at this position, presence of ethyl group (compound **14**) is having highest activity when compared with unsubstituted (compound **1**) and methyl group (compound **2**). Activity is dropped drastically when replaced with bigger steric groups (compounds **16–19**). The same was apparent from MFA discussed earlier. Two electronic descriptors ($ELE/2964$, $ELE/2938$) present same position explains the need of a bulky and electron-withdrawing substituent. Phenyl ring substituted with bromine at this position is bulkier and electron withdrawing in compound **6** shows high activity compared to methyl substitution in compound **2** indicates that bulky linear substituents are necessary at this position. Further, the steric descriptor ($VDW/871$) with negative coefficient present near the *ortho*-position of N^3 -phenyl ring, indicate that any steric group decrease the activity (compound **12** and **13**). When the charge is mapped on the receptor surface model, it shows a negative contour (red color) near the S group of the triazafluorenone ring (Fig. 5). This indicates that an electronegative environment is essential at this position and S fulfills this criterion. Similarly a negative charge is shown near the O present at C^4 of pyrimidone ring. This indicates that an electron-withdrawing group is essential at this position. A blue color contour is observed near to N^3 pyrimidone ring indicating the importance of hydrophobic group is essential at these positions. Hydrogen bonding properties are mapped on the receptor surface as

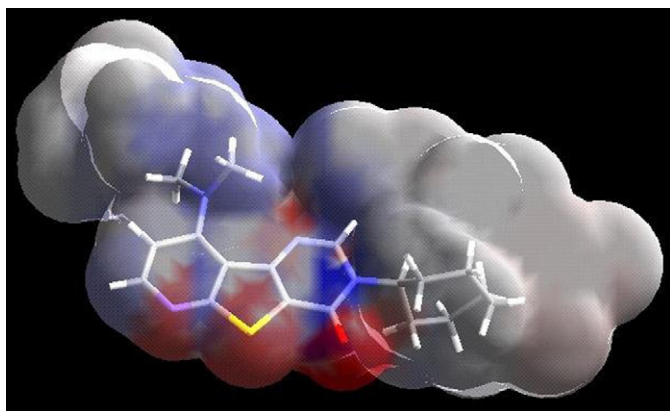


Fig. 5. Receptor surface model with charges mapped on it. Positive regions are shown in blue and negative regions are shown in red. Compound **27** is placed within the generated receptor surface. (For interpretation of the references to color in this figure legend and text citation, the reader is referred to the web version of this article.)

shown in Fig. 6. The figure illustrates that only hydrogen bond acceptor property is observed in receptor surface model. Most of the molecules present in the triazofluorene derivatives are not having hydrogen bond donor groups. Cyan color shows hydrogen bond acceptor properties. The cyan color was seen in close proximity of the pyrimidone N¹, keto-oxygen of pyrimidone, N⁶ of pyridine ring indicating that hydrogen bond acceptor groups are quite essential at these positions. As shown in Fig. 7, brown color indicates the hydrophobic area, while white color indicates hydrophilic area. The hydrophilic region near to pyrimidone N¹, keto-oxygen of pyrimidone, N⁶ of pyridine ring indicate the importance of these groups at these positions. Mapping of hydrophobic region near C³ position of pyrimidone ring explains that substitution of any steric groups at this position increases activity.

The RSA model was further validated using the same test set molecules as in MFA. RSA predicted 100% of molecules

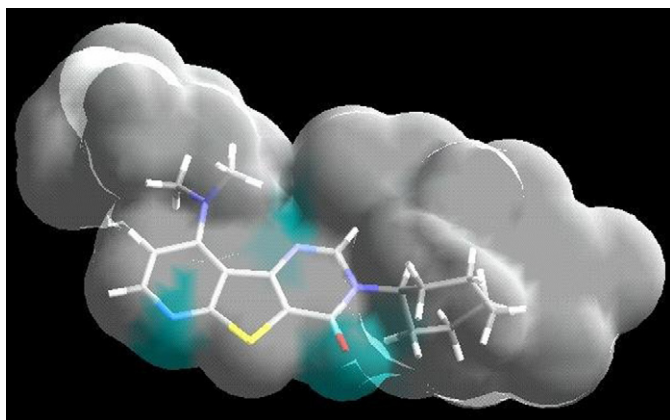


Fig. 6. Receptor surface model with hydrogen bonding property mapped on it. Hydrogen bond donor regions are shown in purple, while hydrogen bond acceptor regions are shown in cyan color. Compound **27** is placed within the generated receptor surface. (For interpretation of the references to color in this figure legend and text citation, the reader is referred to the web version of this article.)

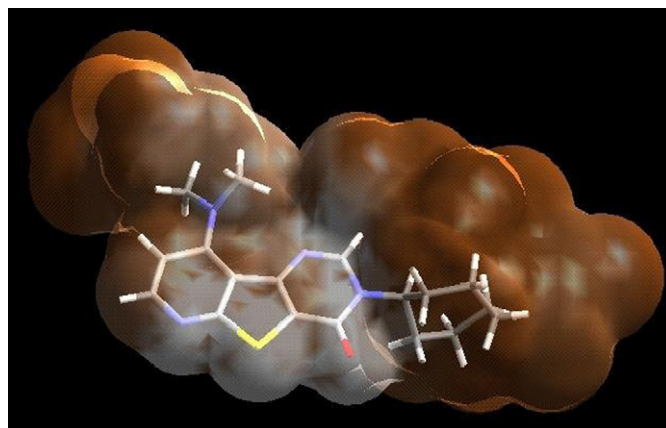


Fig. 7. Receptor surface model with hydrophobic regions mapped on it. Hydrophobic regions are shown in brown and hydrophilic regions are shown in white. Compound **27** is placed within the generated receptor surface. (For interpretation of the references to color in this figure legend and text citation, the reader is referred to the web version of this article.)

correctly with an error less than 1.5. The predictive r^2 (r^2_{pred}) value was found to be 0.776. Hence, the predictive ability of RSM model is also high.

MFA had a higher value of r^2_{cv} of 0.707, while RSA had a lower r^2_{cv} value 0.579. This r^2_{cv} of MFA indicates good internal consistency compared to RSA. In both models, the predictive values fall close to the actual pIC₅₀ values, not deviating more than 1.5 logarithmic unit (Fig. 4(a) and (b); Tables 2 and 3), except for one of the test set molecule (compound **15**) in MFA. Compound **15** is outlier in case of MFA, whereas in RSA, the residual value is 0.310. r^2_{pred} value for MFA is 0.705, while for RSA it is 0.776. Overall both models have good predictive ability while MFA predicted well as compared to RSA.

4. Conclusion

3D-QSAR analyses of 46 triazafluorenone derivatives as inhibitors of mGluR1 were carried out using MFA and RSA models. Comparing these two models, MFA model has better internal predictivity whereas RSA model has better external predictivity. Both models yield significant information to build a strategy to improve the activity of the compounds. Results of MFA and RSA field analysis suggested that electron-donating groups like —NR_2 , —OR , etc. at C⁹ position of triazafluorenone increases the activity and any electron-withdrawing groups at this position decreases the activity. Moderate bulky groups like cyclo-group with pentyl, hexyl, octyl ring or phenyl group with *para*-substituted methyl, ethyl or halides at N³ position of triazafluorenone are essential for mGluR1 inhibitor activity. Moderate groups with electron-withdrawing nature are also favored at this position. Activity is lost with large substituents like cyclooctyl or phenyl group with *para*-substituted higher alkyl groups near N³ position. Overall, the present study investigate the indispensable structural features of the various triazafluorenone analogues which can be exploited

for the structural modifications of these lead molecules in order to achieve improved mGluR1 inhibitory activity.

Acknowledgements

The authors thank Dr. J.A.R.P. Sarma, Senior Vice President and Dr. Rambabu, Senior Scientist, GVK Biosciences Pvt. Ltd. for their cooperation and providing software facilities.

References

- [1] M. Masu, Y. Tanabe, K. Tsuchida, R. Shigemoto, S. Nakanishi, *Nature* (London) 349 (1991) 760–765.
- [2] S. Nakanishi, M. Masu, *Annu. Rev. Biophys. Biomol. Struct.* 23 (1994) 319–348.
- [3] M. Hollmann, S. Heinemann, *Annu. Rev. Neurosci.* 17 (1994) 31–108.
- [4] E. Hermans, R.A.J. Challiss, *Biochem. J.* 359 (2001) 465.
- [5] D.D. Schoepp, D.E. Jane, J.A. Monn, *Neuropharmacology* 38 (1999) 1431–1476.
- [6] J.P. Pin, R. Duvoisin, *Neuropharmacology* 34 (1995) 1–26.
- [7] K. Walker, M. Bowes, M. Panesar, A. Davis, C. Gentry, A. Kesingland, F. Gasparini, F. Spooen, N. Stoehr, A. Pagano, P.J. Flor, I. Vranesic, K. Lingenhoebl, E.C. Johnson, M. Varney, L. Urban, R. Kuhn, *Neuropharmacology* 40 (2001) 1–9.
- [8] S. Litschig, F. Gasparini, D. Rueegg, N. Stoehr, P.J. Flor, I. Vranesic, L. Prezeau, J.P. Pin, C. Thomsen, R. Kuhn, *Mol. Pharmacol.* 55 (1999) 453–461.
- [9] J. De Vry, E. Horvath, R. Schreiber, *Eur. J. Pharmacol.* 428 (2001) 203–214.
- [10] M. Okada, M. Takahashi, S. Hayashibe, *PCT Int. Appl.*, 1999, WO 9944639.
- [11] B.C. Van Wagenen, S.T. Moe, D.L. Smith, S.M. Sheehan, I. Shcherbakova, R. Travato, R. Walton, R. Barmore, E.G. Delmar, T.M. Stormann, *PCT Int. Appl.*, 2000, WO 2000073283.
- [12] A. Binggeli, H. Maerki, V. Mutel, M. Wilhelm, W. Wostl, *PCT Int. Appl.*, 2002, WO 2002051418.
- [13] B.P. Clark, J.R. Harris, A.E. Kingston, *PCT Int. Appl.*, 2000, WO 2000026199.
- [14] S.J. Ambler, S.R. Baker, B.P. Clark, D.S. Coleman, R.J. Foglesong, J. Goldsworthy, G.E. Jagdmann, K.W. Johnson, A.E. Kingston, W.M. Owton, D.D. Schoepp, J.E. Hong, J.M. Schkeryantz, M.S. Vannieuwenhze, M.S. Zia-Ebrahimi, *PCT Int. Appl.*, 2001, WO 2001032632.
- [15] F. Micheli, R. Di Fabio, F. Bordini, P. Cavallini, P. Cavanni, D. Donati, S. Faedo, M. Maffei, F.M. Sabbatini, G. Tarzia, M.E. Tranquillini, *Bioorg. Med. Chem. Lett.* 13 (2003) 2113–2118.
- [16] G.Z. Zheng, P. Bhatia, J. Daanen, T. Kolsa, M. Patel, S. Latshaw, O.F. El Kouhen, R. Chang, M.E. Uchic, L. Miller, M. Nakane, S.G. Lehto, M.P. Honore, R.B. Moreland, D. Jorge, R.B. Moreland, J.D. Brioni, A.O. Stewart, *J. Med. Chem.* 48 (2005) 7374–7388.
- [17] G.Z. Zheng, P. Bhatia, T. Kolsa, M. Patel, O.F. El Kouhen, R. Chang, M.E. Uchic, L. Miller, S. Baker, S.G. Lehto, M.P. Honore, J.M. Wetter, K.C. Marsh, R.B. Moreland, J.D. Brioni, A.O. Stewart, *Bioorg. Med. Chem. Lett.* 16 (2006) 4936–4940.
- [18] A. Golbraikh, A.J. Tropsha, *J. Mol. Graph. Model.* 20 (2002) 269.
- [19] Cerius2 Molecular Modeling Program Package, Accelrys; Scranton Road, San Diego, CA 92121–93752, USA <http://www.accelrys.com/>.
- [20] J. Gasteiger, M. Marsili, *Tetrahedron* 36 (1980) 3219–3228.
- [21] D. Rogers, A.J. Hopfinger, *J. Chem. Inf. Comput. Sci.* 34 (1994) 854–866.